Investigation of Observation Quality Parameters for H.E.S.S.-II

Masterarbeit aus der Physik

Vorgelegt von
Maximilian Schandri
05.03.2018

Erlangen Centre for Astroparticle Physics
Friedrich-Alexander-Universität
Erlangen-Nürnberg

Betreuer: Prof. Dr. Stefan Funk

Abstract

The High Energy Stereoscopic System (H.E.S.S.) is a telescope array, which detects cosmic gamma-rays (γ-rays). These particles interact with the earth's atmosphere and produce an electron-positron shower. From these secondary particles the emitted Cherenkov light is detected. In the first phase, the instrument consisted of four telescopes. The observations are subject to the errors of hardware and the nature of the weather. Because of that the quality of the data varies. In order to only extract high quality data, a selection needs to be performed. For the first phase this selection was optimized.

In the second phase of H.E.S.S. a fifth telescope was added to the array. Since the new telescope is larger and has different properties than the small telescopes, the data quality selection needs to be readjusted. The first step was done in this thesis. The selection criteria of the first phase were analyzed and it became clear that it was necessary to adapt the broken pixel criterion. For this purpose, simulations of gamma events were studied dependent on the number of disabled pixels. The resulting upper limit on the number of broken pixels is 275 pixels. Furthermore the transparency coefficient (TC), measuring the opacity of the atmosphere, was calculated for the second phase. It turned out that for the TC the same limits as for the first phase can be taken. Lastly, the new insights on the data selection were tested on a flux analysis of the Crab Nebula, which confirmed the positive effect of the criteria on the data quality.

Contents

1. Introduction **6**
1.1. Gamma-ray Astronomy 6
1.2. High Energy Stereoscopic System 7

2. Runselection of H.E.S.S.-I **10**
2.1. Detection Criteria Set 10
2.2. Spectral Criteria Set 10

3. Detection Criteria for H.E.S.S.-II **12**
3.1. Finding the Broken Pixel Cut 14
3.2. Distribution of Broken Pixels of CT5 15
3.3. Energy Bias 15
3.4. Efficiency 17
3.5. 68% Quantile of the Point Spread Function 18

4. Spectral Criteria for H.E.S.S.-II **21**
4.1. Transparency Coefficient 21
4.2. Calculating the Transparency Coefficient 23

5. Application of the Quality Selection to Data **26**

6. Conclusion **28**

A. Detection Parameter Plots **29**

B. Fits **30**
B.1. Unweighted Quantities 30
B.2. Weighted Quantities 30

C. Rate versus Zenith Angle **32**

1. Introduction

1.1. Gamma-ray Astronomy

For a very long time astronomers want to know what happens in the Universe. γ-ray astronomy is one possible way to answer fundamental questions. One question is, where the origins of the cosmic radiation (CR) are. The main components of the CR reaching the earth's atmosphere are protons and heavier nuclei. These particles are accelerated in neuron stars, solar-mass black holes, other galaxies or active galactic nuclei [6]. It would be convenient to use these particles to get a better understanding of the source. However, a big disadvantage is that they are charged and thus deflected by magnetic fields in the cosmos. This change of the direction is not negligible, since the curvature radius of a particle in the interstellar magnetic fields with an energy of 1 PeV ($\hat{=} 10^{15}$ eV) is about one light year. This is smaller than the distance to the closest star and with lower energies this radius becomes even smaller [8]. Thus the directional information is lost. High energetic photons, so called *γ-rays*, are produced if, for instance, protons interact with magnetic fields, starlight, cosmic background or with surrounding material [8]. γ-rays are uncharged because of this they can be used to identify their sources. This is exemplified in figure 1.1. Since γ-rays have a similar energy distribution as the original charged particles [8], another question they can answer is what the spectrum of the accelerated particles is.

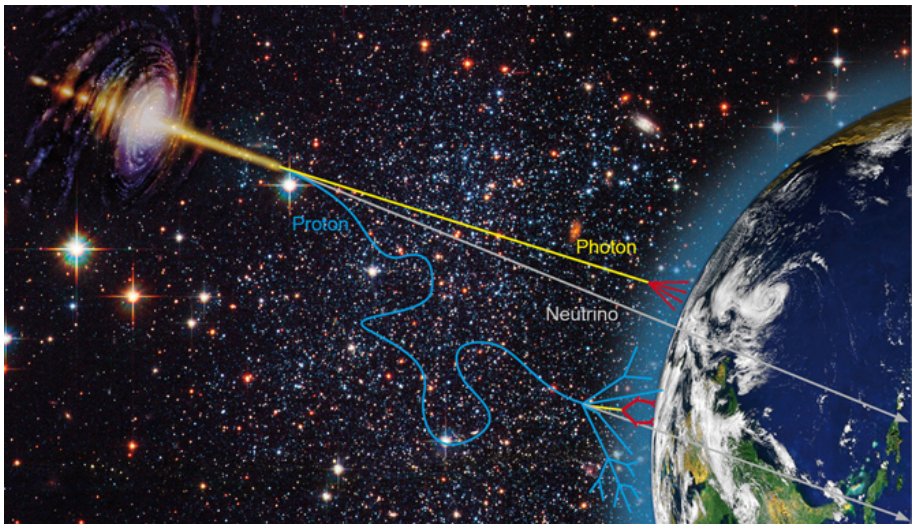

Figure 1.1: Illustration of the path messenger particles take before they reach the earth. Charged particles, like protons, are deflected in the interstellar magnetic field, while uncharged particles (photons, neutrinos) are not. Protons and photons interact with the earth's atmosphere, whereas for neutrinos the most probable path is right through the earth without interactions. Image taken from [9].

To be able to acquire information about their origin, these particles need to be detected first. It is convenient to use space-based detectors because γ-rays are absorbed by the earth's atmosphere. These detectors are present for the low energy regime. One example of a space-based detector is the Fermi Large Area Telescope, which has an observation energy range from 30 MeV to 300 GeV [6]. The spectrum of γ-rays follow a power-law, which means that the number of photons decreases rapidly for increasing energy. For energies larger than 100 GeV the detection area of space-based instruments becomes insufficient and ground-based telescopes are needed. The idea is to detect secondary particles produced by the interaction between γ-rays and the atmosphere, which is indicated as red lines in the earth's atmosphere in figure 1.1. The dominant interaction for γ-rays is the production of electron-positron pairs. These secondary particles send out *Cherenkov light*, which can

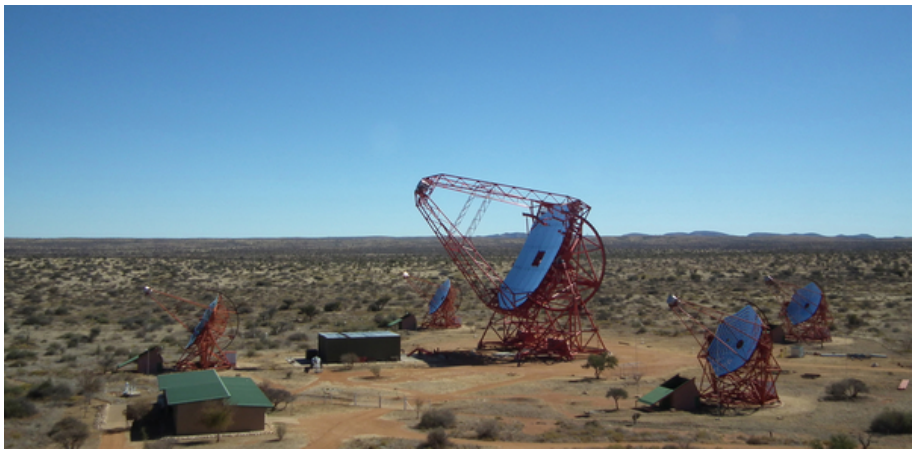

Figure 1.2: The H.E.S.S. telescope array with all five telescopes. Four small telescopes in a square formation with the larger telescope in the middle.

be detected on the ground. The conditions for a particle to emit Cherenkov light are: it is charged and its velocity v is higher than the speed of light in a given material with refractive index n. This light is send out in an angle of

$$\cos\Theta_C = \frac{1}{\beta n}$$

with $\beta = v/c$, which is about 1 ° in air. A high energy photon interacts with the atmosphere at an altitude of 10-20 km. The resulting Cherenkov light cone lights up an area of about 50000 m^2. Gamma energies of one TeV result in an intensity of about 100 photons per square meter [8]. To be able to detect showers of such a low intensity, large mirror areas are needed to collect enough light for a camera. There are various projects which work with ground-based telescopes to detect γ-rays, such as the MAGIC-Instrument (La Palma), the VERITAS-Telescope (Arizona) and the H.E.S.S.-System (Namibia). They all have a similar functionality. In this thesis only the last-named telescope will be described in detail.

1.2. High Energy Stereoscopic System

The High Energy Stereoscopic System is an arrangement of *Cherenkov telescopes* (CT). This project had two phases: The first phase H.E.S.S.-I started in summer of 2002 with the activation of one of the four medium sized telescopes, which are subsequentially called CT1-4. These telescopes are arranged in a square with 120 m side length. This is a trade-off between a good stereoscopic viewing of the showers and the necessity that one shower is seen by two or more telescopes. The hardware components are the mirror, the camera, the mounting and the electronics to readout the data and supply the camera with electricity. The mirror is split in 382 small circular mirrors with a radius of 30 cm, which results in a total mirror area of 108 m^2 for each telescope. The camera consists of 960 photo-multiplier tubes (PMT), which are divided into groups of 16 PMTs, so called *drawers*. Drawers are physically joined together. This must not be confused with the sector of a camera, which is a group of 64 pixels. These sectors are used for the second layer of the trigger system. There are 38 overlapping sectors for each camera. The trigger system has three steps:

1. single pixel: threshold of 4 photoelectrons (p.e.) in 1.5 ns
   → triggered pixel

2. sector: coincidence of 3 triggered pixels
   → triggered telescope

3. if operating in stereo mode: coincidence of two telescopes triggering within 80 ns
   → only individually triggered telescopes are read out

The *trigger rate* of a telescope is the frequency with which it registers showers. The triggered signals of each PMT are stored in two analogue ring sampler (ARS) circuits, for high and low gain to have a large dynamical range [1].
In the second phase H.E.S.S.-II of the project which began in summer 2012, a fifth telescope called CT5 started taking data. CT5 is located in the center of the squared arrangement of H.E.S.S.-I. Its mirror has a total area of 614 m^2, is divided into 875 hexagonal facets and reflects the Cherenkov light to a camera with 2048 pixels. Another difference of CT5 to the small telescopes is the mono analysis, which has a higher sensitivity if done with CT5 than with CT1-4. Here, as the name already states, the analysis is performed only with the data of CT5. In figure 1.2 the telescope array with all five instruments can be seen.
In reality not every observation has the same quality because of different weather conditions or the condition of the hardware. It is important to filter out data with inferior quality, to be able to perform adequate analysis. However, not only the quality, but also the quantity is important for the analysis. Because of this it is crucial not to set the constraints for the quality too hard. In the following this data selection for H.E.S.S.-I is described, since for H.E.S.S.-II this was not yet done analytically. The first step is done in this thesis.

For the first part of this thesis the state of the art of the data quality selection for H.E.S.S.-I is described. On the basis of the criteria of H.E.S.S.-I the decision which criteria need to be adjusted for H.E.S.S.-II was made. For this purpose the detection criteria, which are described in the following chapter, were studied. Thereby the need of adjusting the broken pixel criterion, became apparent. For that reason, the effect of disabled pixels on simulations of γ-events will be investigated to obtain a suitable broken pixel limit for CT5. Thereafter the spectral criteria are viewed, but the focus is on the TC. It will be explained in detail and afterwards calculated for CT5. With the help of the flux of the Crab Nebula, the new obtained cut on the number of broken pixel and results from the TC, the computation will be discussed. The conclusion summarizes the achieved work and gives a short outlook for further studies of the quality selection of H.E.S.S.-II.

2. Runselection of H.E.S.S.-I

The runselection of H.E.S.S.-I is already optimized and will be described in this chapter. The recorded shower events are taken in segments called *runs*, which are usually 28 minutes long. In a database all important additional data is saved for a given run. For example the length of the observation, the condition of the cameras and the number of registered showers. This additional data is used to reject runs of inadequate quality.
In this selection a trade-off between high quality and enough statistic needs to be found. There are two levels of runselection. The first one is called *detection* and the second one *spectral*. Each level consists of a set of criteria which need to be fulfilled. The goal of the spectral criteria set is to generate a good spectrum of a source. To do so, the energy reconstruction is important. For H.E.S.S. this is done via simulated effective areas and lookup tables. Runs where the atmospheric conditions are close to those of the simulations, will have adequate reconstructions. For the detection data quality selection no spectrum is needed. Here, high statistics are important to be able to assure the detection of showers from the source. In other words, large numbers of runs are needed to perform advantageous analyses. The information about the runselection of H.E.S.S.-I is taken from [7].

2.1. Detection Criteria Set

To gain high statistics only hardware quantities are considered in the detection criteria set. These can be separated into three groups:

- Run Duration (1)
- Camera (3)
- Tracking Parameters (4)

The number in brackets indicates how many single criteria are in each group. This means, there are eight parameters which are checked. In table 1 these parameters are listed with their limits. The camera and tracking cuts are applied for each telescope individually and will only exclude single telescopes. If one or no telescope of a run is left after the cuts, this run will be filtered out. A run is also rejected if the duration of a run is outside of the allowed range. Brief explanations of the parameters are listed in the following paragraph. Detailed information can be looked up in [7].
The *participation fraction* of a telescope shows the contribution percentage on the triggered events. A telescope needs to participate in at least 40% of the events to pass this cut. The broken pixel of a camera are distinguished by the reason why they are broken. The reasons for *hardware broken* pixels can be that there was no signal measured in the PMT photocathode or the ARS was defect. Other problems, like lack of high voltage (HV), require a hardware expert on site, who manually removes a pixel for a longer time. These pixels are marked as *HV switched off*. The limit on the *deviation in Ra/Dec* (Ra: Right ascension, Dec: Declination) ensures that the absolute tracking position is correct, whereas the cut on the root mean squared (RMS) of the *deviation in Az/Alt* (Az: Azimuth, Alt: Altitude) checks that the tracking of the telescope runs smoothly.

2.2. Spectral Criteria Set

For the measurement of a spectrum the energy reconstruction is important. The registered Cherenkov photons in a shower are directly correlated with the energy of the initial γ-ray. By clouds or other air contaminations like dirt from the desert, Cherenkov photons can be absorbed. If the absorption is weak and constant over the whole run, the real photon count can be estimated with a good calibration. Clouds or fog patches moving into the field of view (FoV) of the telescopes while data is taken, will result in a variable trigger rate.

Type	Parameter	Lower Limit	Upper Limit
Detection	Duration [s]	600	7200
	Participation Fraction	0.4	1
	Hardware Broken Pixel	0	120
	HV switched off Pixel	0	50
	Ra Deviation Mean [degree]	-0.01667	0.01667
	Dec Deviation Mean [degree]	-0.01667	0.01667
	Az Deviation RMS [arcsec]	0	10
	Alt Deviation RMS [arcsec]	0	10
Spectral	δ_1 [% of mean val.]	-30	30
	δ_2 [% of mean val.]	0	10
	Transparency Coefficient	0.8	1.2

Table 1: Both run selection sets for H.E.S.S.-I with its parameters and limits. The detection set is separated in its groups: Run Duration, Camera, and Tracking Parameters.

For instance, if a large cloud is entering the FoV, the trigger rate will steadily decrease, whereas small clouds moving through the FoV will effect the trigger rate on a smaller timescale. The spectral criteria set adds three conditions to the detection criteria set, to filter out all runs with variable trigger rate. These three additional parameters are:

- δ_1: relative change in the system rate
- δ_2: root mean square divided by the mean of the system rate
- Transparency Coefficient

These parameters show the stability of the system rate over the whole run (δ_1) and on a smaller timescale (δ_2). A detailed explanation can be found in [7]. The transparency coefficient is used for long term trigger rate evolutions. It is a measure for the opacity of the atmosphere. Before this parameter was used the system trigger rate versus the run date was fitted. The obtained fit function gave an estimate of the system trigger rate for a given time. A run with a system rate lower than 80% of the value predicted by the fit function to the given run date, was filtered out. This method became unusable because of hardware adjustments which modified the trigger rates. One of these adjustments was the renewal of the mirrors. Here, the trigger rates fluctuated on too small timescales to obtain acceptable estimations. Because of that the TC was introduced in the quality selection to replace the old method. It is less hardware dependent and is defined in detail later in this thesis.

In the next chapter the detection criteria for H.E.S.S.-II are studied to see if new adjustments are needed.

3. Detection Criteria for H.E.S.S.-II

The first step to find suitable detection criteria limits for H.E.S.S.-II, was to look at the cut parameters, which are used for H.E.S.S.-I data (see tab. 1). The distributions shall illustrate the impact of adjusting the limit on the number of rejected runs. In figure 3.1 the duration, the participation fraction of CT5, the HV switched off pixels of CT5, and the mean Dec deviation are shown. The step histogram (blue line) is filled with all available runs, in which CT5 was active. In the filled histogram (orange) only the runs which suit the detection quality, set for H.E.S.S.-I without the restrain on the plotted parameter, are counted. Considering the case of the duration, the filled histogram contains all runs which fulfill all detection cuts except the limit on the duration. The limit on the participation fraction is the only parameter which was adjusted for H.E.S.S.-II because of the higher trigger rate for CT5 in relation to the small telescopes. This adjusted cut distinguishes between CT1-4 and CT5. For CT1-4 the modified allowed range of the participation fraction value is $[0.04 - 1]$ and for CT5 it is $[0.5 - 1]$. For CT5 this new range is shown in figure 3.1 on the top right. The dashed lines with numbers displaying their position, show the limits on the given parameter. For example on the top left in figure 3.1 the distribution of the duration is shown. The minimum duration is 600 seconds and the maximal allowed value is 7200 seconds. The two dashed thin lines without numbers indicate the range of the histogram. Bins outside the enclosed range are under- and overflow bins. All values outside of the dashed lines are filled in these two bins.

These plots show that most of the parameter distributions are narrow or are already well filtered by the other quality criteria. This is also true for the rest of the parameters, which are shown in the appendix A. Only the duration and HV switched off pixels distributions are wider than the others in relation to the limits set for H.E.S.S.-I. The minimum value for the run duration is needed to guarantee enough statistics and therefore just the detection criterion for broken pixels will be investigated for H.E.S.S.-II in this thesis. Another reason to study this criterion is because the camera of CT5 is significantly larger than the cameras of H.E.S.S.-I. If the limit can be put to slightly higher values, the number of runs passing this criterion will increase more than for any other criterion. More runs imply higher statistics and thus better analysis can be performed.

The initial idea was to look at how the cut on the number of broken pixels was set for H.E.S.S.-I and then repeat it with data of H.E.S.S.-II. For the first phase of the telescope it was obtained by a study on the muon efficiency. This quantity is a measure of the loss of information about the light inside the telescope. Here instead of γ-ray shower events, muon events are examined because detected muon showers are seen as a ring on the image. From the ring radius and an azimuthal intensity profile, the number of photons, generated by the muon can be calculated [5]. This study was done by O. Bolz in 2004 (see [3]). For this Monte-Carlo simulations were used. For the first phase of the instrument a clear cut was seen for 12 disabled pixels on the ring, which can be seen in figure 3.2. The black points show the efficiency obtained with a random homogeneous generated distribution of disabled pixels over the whole camera. For the red dots the distribution of inactive pixels were taken from real data and applied to the simulations. The effect is the same for both cases. The 12 disabled pixels on the muon ring correspond to 120 disabled pixels on the whole camera. The attempt to also see this clear step for H.E.S.S.-II can be seen in figure 3.3. Here only a homogeneous generated distribution of disabled pixels was used and since the CT5 camera is larger than the cameras of H.E.S.S.-I the maximum number of disabled pixels is set higher. Only a constant increase is present and no defined step is seen. The reason why there is a clear step for H.E.S.S.-I, is the used selection criteria on the muon events. This selection was optimized for muon showers and can be looked up in [3]. Since the broken pixel cut should be valid for γ-ray events this idea was not further researched. Because of that a different way to set the broken pixel limit was needed.

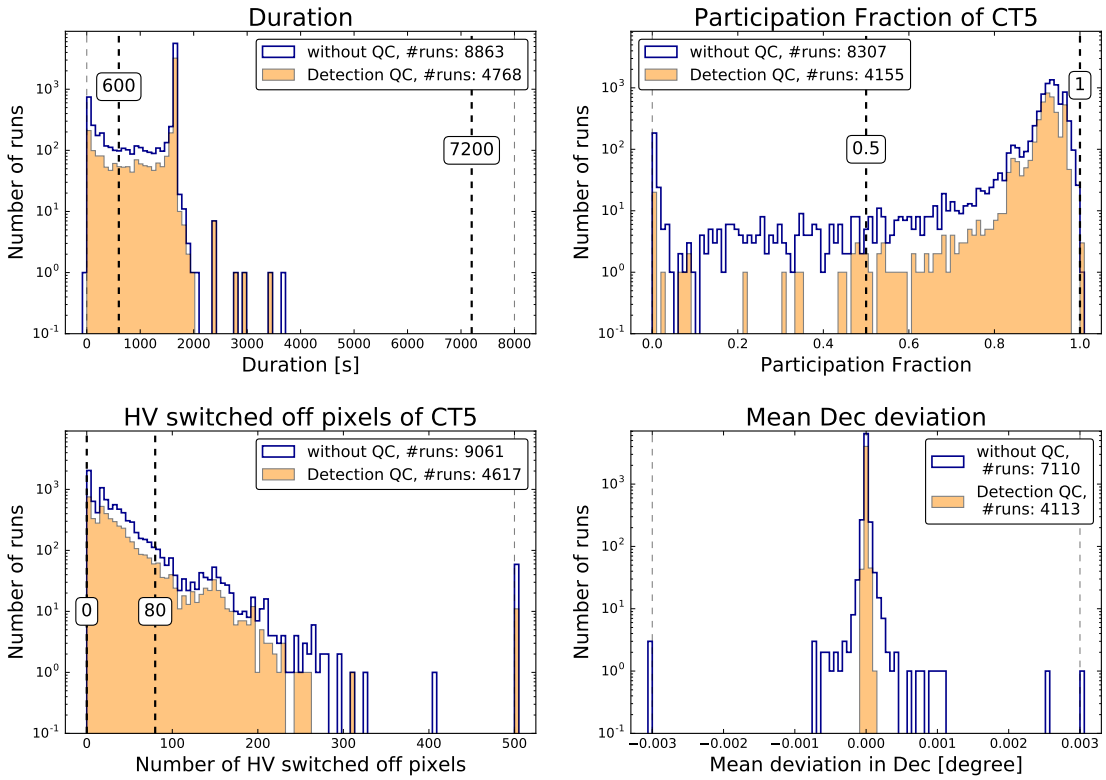

Figure 3.1: Example detection parameter distributions of H.E.S.S.-II runs. The step histogram (blue) shows all runs without quality cuts. In the filled histogram (orange) all runs are counted which fulfill all detection quality cuts, except the cut on the plotted parameter. The dashed lines with numbers indicating the position show the currently used limits on the given parameter. The thin gray dashed lines (without numbers) show the limit of the histogram. The bins outside of the thin lines are under- and overflow bins. For the plot on the bottom right no lines which show the limits are seen because the limits are out of range for this plot.

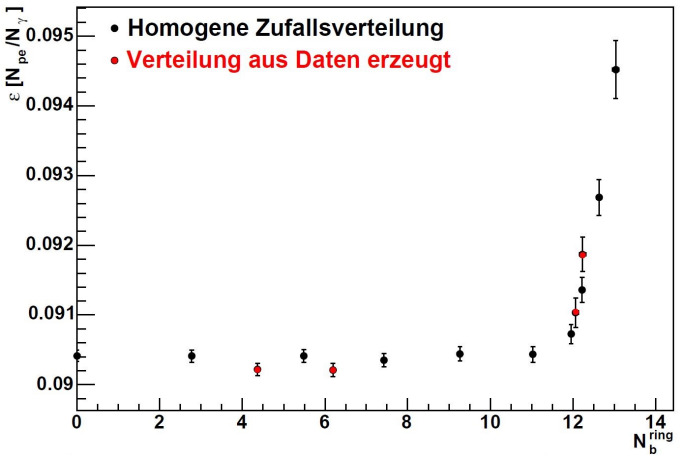

Figure 3.2: Muon efficiency calculated from Monte-Carlo simulations. On the x axis the mean number of disabled pixels on the muon ring is shown. On the y axis the muon efficiency is shown. The black points are generated via a homogeneous distribution of disabled pixels. For the red circles a distribution of broken pixels from real data was taken and applied to the simulations. Image taken from [3].

The effect of broken pixels on the H.E.S.S.-II camera was investigated using simulations of γ-ray events. The real distribution of broken pixels on the camera is assumed to lie between a random distribution of single pixels and a distribution with entire groups of switched off pixels. Therefore two studies were made. For the first one arbitrary pixels were selected and switched off before the final image cleaning. The second one was done in the same way with the only difference that instead of arbitrary pixels, arbitrary drawers were selected. To disable the chosen pixels, their intensity was set to zero. Various quantities were computed dependent on the number of disabled pixels to find a suitable limit.

3.1. Finding the Broken Pixel Cut

For all 200 gamma simulation runs the same pixels or drawers were disabled. In the case of single pixels this was done in steps of 50, from 0 to 500. Disabling drawers was done in steps of 2 (= 32 pixels), from 0 to 480 pixels. The reason why the steps for pixels are larger than for drawers is the assumption that disabled pixels randomly distributed over the camera have a smaller effect than a group of pixels.
Three quantities were selected to set and discuss a new limit of the broken pixel criteria:

- Energy bias: setting the limit
- Efficiency: evaluate the limit
- 68% Quantile of the point spread function: evaluate the limit

The quantities are calculated based on the simulation runs, in which all runs have the same number of disabled pixels. The case that for an analysis all runs have the same number of disabled pixels is highly unlikely, unless the analysis is done with very few runs. The more probable case is that the runs have different numbers of broken pixels. In the following section the distribution of broken pixels for real data is shown. The simulation data can then be weighted with this distribution to obtain a more realistic view on the studied quantities.

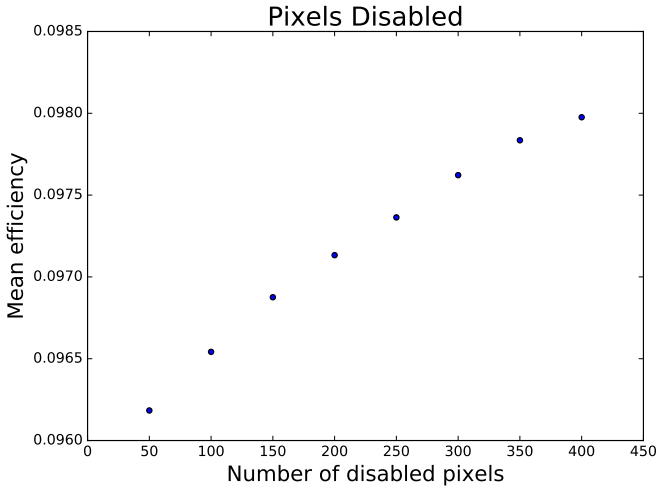

Figure 3.3: Muon efficiency calculated from Monte-Carlo simulations for the second phase of the telescope system.

3.2. Distribution of Broken Pixels of CT5

The distribution of the sum of broken and HV switched off pixels is needed because for the simulation analysis it was not distinguished why pixels were shut off. The only constraint on the data used for this plot was that the run number shall be greater than 95000 because the high voltage supply of the CT5 camera has been adjusted at this time.
The distribution is shown in figure 3.4. The second bin is the dominant one, considering the logarithmic y axis. For increasing number of broken pixels up to ~ 350 pixels there is an exponential decrease in number of runs. The plot does not show all possible broken pixel values because there are also runs with the maximum number of broken pixels of 2048. For the weighting, the whole range of broken pixels was taken into account.

3.3. Energy Bias

One result of the analysis of the data is the energy of a shower. This can be estimated by the number of photons registered inside the shower cone. The *energy bias* is a measure for how much the reconstructed energy E_{rec} differs from the simulated energy E_{true}. It can be calculated by

$$E_{\text{bias}} = \frac{E_{\text{rec}} - E_{\text{true}}}{E_{\text{true}}}$$

It is desirable that E_{bias} is as close to zero as possible because this would state that the reconstruction of the energy results in the correct true energy. For one given number of disabled pixels and drawers (n), it was calculated separately for every event (i) and then averaged.

$$E_{bias,n} = \frac{1}{k} \cdot \sum_{i=1}^{k} \frac{E_{\text{rec,i}} - E_{\text{true,i}}}{E_{\text{true,i}}} \tag{1}$$

Where k is the number of registered events. The energy bias relative to that obtained for zero disabled pixels is studied, to focus on the deterioration of their quantity. Figure 3.5a shows that it decreases with increasing number of disabled pixels as well as for drawers. This means that the reconstructed energy decreases because it is calculated on the basis of how many photons are registered inside the shower. Considering that fewer pixels are available for higher number of disabled pixels, the number of photons taken for the energy

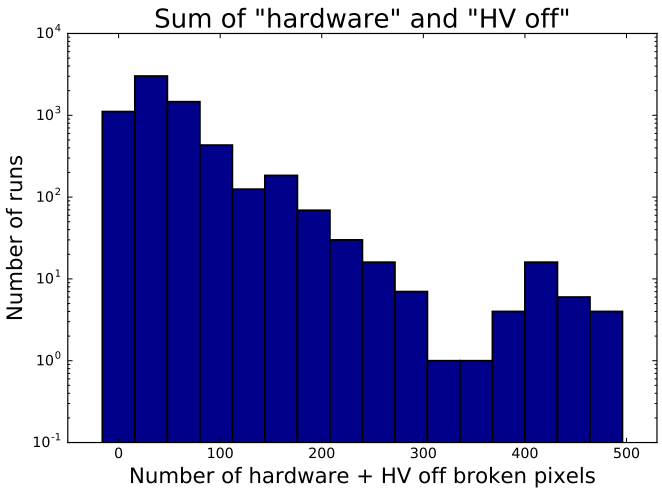

Figure 3.4: Distribution of the sum of "hardware" and "HV off" broken pixels for CT5 obtained from real data. The bin centers range from 0 pixels to 480 pixels to match the range of disabled drawers.

calculation also decreases.

For a standard spectrum analysis it is usually required that the energy bias is not worse than 10%. With this threshold and two linear fits to the data for disabled pixels and drawers respectively the cut for broken pixels is obtained. For a linear fit function

$$f(x) = m \cdot x + t \tag{2}$$

where f is the energy bias given in eq. (1) and x corresponds to the number of disabled pixels. The fit parameters can be seen in table 2. The corresponding plots are shown in the appendix B.2 (see fig. B.1). The resulting number of pixels values for a maximum worsening of 10% are 271 ± 6 for pixels and 310 ± 9 for drawers. The errors can be calculated via Gaussian error propagation (see appendix B.1, eq. (10)).

The fact that the drawer limit is higher than the one for pixels may seem strange at first, but can be explained as follows. Consider an equal number of pixels is disabled for the same event, one time random single pixels and the other time whole drawers are deactivated. In the case of random single pixels the shower can likely still be reconstructed by the analysis software, but since pixels are missing the energy reconstruction is poor. For the other case this shower may be sorted out because the analysis cannot recognize the shower, and only events with fewer disabled pixels in the shower itself are taken into account. Thus the energy reconstruction can be superior. Since for real data the distribution is assumed to be between random single pixels and drawers, the new cut should be between those two values. To be on the safe side it should stay closer to the smaller value. $\Rightarrow$ **275 pixels**
In figure 3.5b the weighted relative energy bias is shown. Here E_{bias} is summed up to each disabled pixel value n (eq. (3)). The obtained values were fitted by eq. (4) and the resulting fit parameters can be seen in table 3.

$$\bar{E}_{\text{bias}} = \frac{\sum_0^n E_{\text{bias,i}} \cdot w_{\text{i}}}{\sum_0^n w_{\text{i}}} \tag{3}$$

where w_{i} is the weighting for i disabled pixels.

$$f_{fraction}(x) = \frac{a}{x+b} + c \tag{4}$$

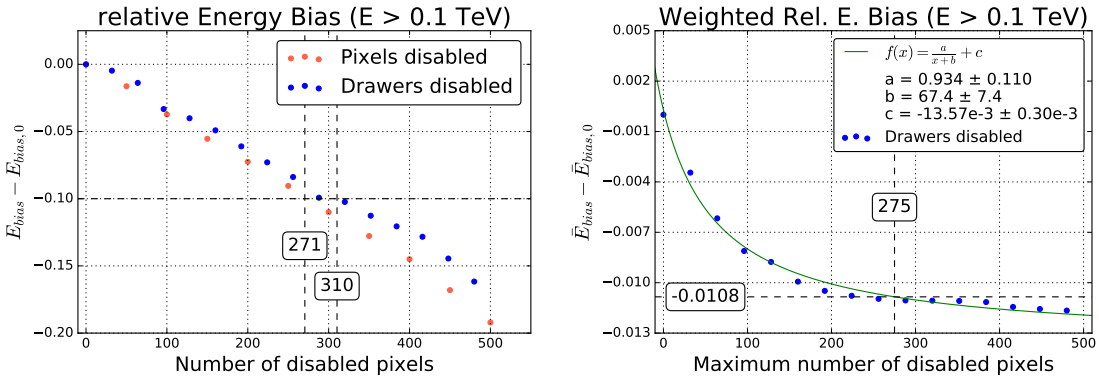

(a) Worst case.

(b) Fit of the weighted distribution.

Figure 3.5: Relative energy bias for energy threshold of 0.1 TeV. $E_{\text{bias},0}$ is the energy bias for zero disabled pixels.

For the cut at 275 pixels the energy bias is $(1.08 \pm 0.06)\%$ poorer than for zero disabled pixels. The error was again calculated with the Gaussian error propagation (see appendix B.2, eq. (12)). The new broken pixel cut is strengthened by the fact that the weighted relative energy bias flattens for increasing maximum number of disabled pixels because small variations on the cut limit result in small variations on the value for the weighted relative energy bias.
The other two quantities (efficiency and 68% quantile of the PSF) introduced above help to evaluate whether this limit is reasonable or not. There are two cases: the worst case that every run has the same number of broken pixels and a more realistic one, where a maximum number of broken pixels is given and all runs with fewer broken pixels are also taken into account. For the second case the distribution of broken pixels from real data is needed to weight the values, like it was already done for the relative energy bias.

3.4. Efficiency

A basic characteristic of the telescope, which can be influenced by the number of broken pixels, is how many showers the analysis software can register. This characteristic is called *efficiency*. If more pixels are switched off, there is less data and the probability that a shower will successfully be analyzed decreases. This behavior can be seen in figure 3.6. Here all events with a reconstructed energy greater than 0.1 TeV are counted. It was normed to the value obtained with no pixels disabled.
Figure 3.6a shows that if, for example, 500 random pixels are disabled for every simulation run the loss of registered showers is about 30%. The vertical dashed line at 275 disabled pixels marks the new cut value and the horizontal line at 0.84 is the combined result of two fits. The corresponding plots can be seen in the appendix B.2 (fig. B.2). For drawers and pixels a linear fit (see eq. (2)) was performed to determine the efficiency for 275 broken pixels. For drawers it is 0.836 ± 0.011 and for pixels it is 0.841 ± 0.004. The errors are calculated from the uncertainties of the fit which can be seen in table 2. The formula of the error is shown in the appendix B.1 (eq. (11)). For overview reasons and because they are so close to each other, these two values are shown as one horizontal line at 0.84 in the figure. In other words, for the case that all runs have 275 disabled pixels, $\sim$**16%** fewer events are found than for zero disabled pixels.
In figure 3.6b the weighted efficiency, calculated as for the relative energy bias, is shown. The fit was performed with the same function as for the weighted relative energy bias (eq. (4)) and the resulting fit parameters are shown in table 3. The corresponding weighted

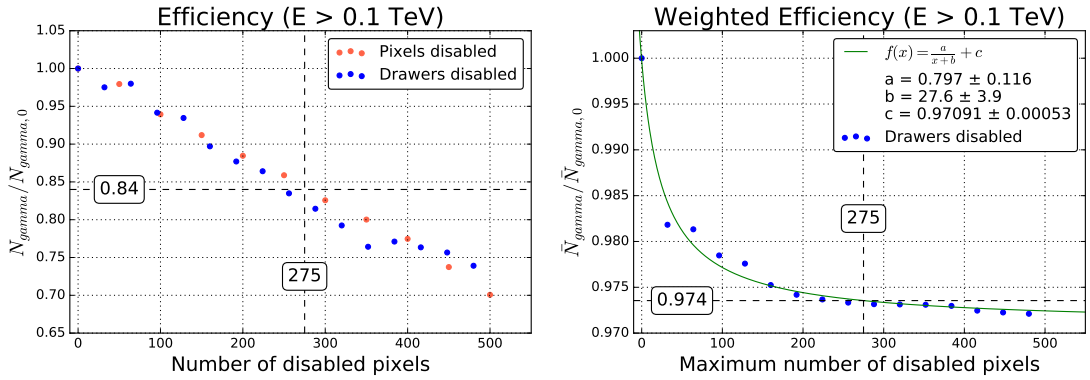

(a) Normalized to the value for zero disabled pixels.

(b) Weighted with the real distribution.

Figure 3.6: γ-ray efficiency for an energy threshold of 0.1 TeV. $N_{gamma,0}$ is the efficiency for zero disabled pixels.

efficiency for 275 disabled pixels is 0.9735 ± 0.0008, where the error is obtained with eq. (12). In this more realistic case because of the weighting with a real distribution of broken pixels obtained from observation runs, the loss of events relative to zero disabled pixels is **$\sim$3%**.

3.5. 68% Quantile of the Point Spread Function

Every successfully analyzed γ-event has a reconstructed direction ($\overrightarrow{v}_{\text{rec}}$) that may vary from the true position of the simulated source ($\overrightarrow{v}_{\text{true}}$). The directions are stored in Alt/Az coordinates and are transformed into Cartesian coordinates, to calculate the angle between event and true position. The distribution of this angle for one source is called Point Spread Function (PSF). The lengths of the resulting vectors are set to one. The angle can then be calculated by

$$\Theta = \arccos\left(\frac{\overrightarrow{v}_{\text{true}} \cdot \overrightarrow{v}_{\text{rec}}}{|\overrightarrow{v}_{\text{true}}| \cdot |\overrightarrow{v}_{\text{rec}}|}\right) = \arccos(\overrightarrow{v}_{\text{true}} \cdot \overrightarrow{v}_{\text{rec}})$$

It is conventional to look at the squared angle, which can be seen exemplary for 50 disabled pixels in figure 3.7a. The majority of events is located at small angles. Therefore the distribution is shown in this range in figure 3.7b. The dashed lines again mark the end of the histogram. The width of this distribution is determined with its *68% quantile*. It is the Θ^2 value for which 68% of the values are smaller. For a good reconstruction this value is small. It is expected to increase with larger numbers of disabled pixels.
In figure 3.8a the quantile is plotted against the number of disabled pixels for the cases of randomly disabled drawers and pixels. The effect of disabling random pixels is almost not visible. Disabling drawers has a much greater influence. For both data sets a linear fit was done and the resulting quantiles for 275 broken pixels are for drawers $0.0601 \pm 0.0015\,\text{deg}^2$ and for pixels $0.0423 \pm 0.0004\,\text{deg}^2$. The 68% quantile of the distribution for zero disabled pixels is $0.0416\,\text{deg}^2$. This means that for 275 random disabled pixels the distribution gets **$\sim$2%** wider in relation to zero, whereas the broadening for disabled drawers is **$\sim$44%**.

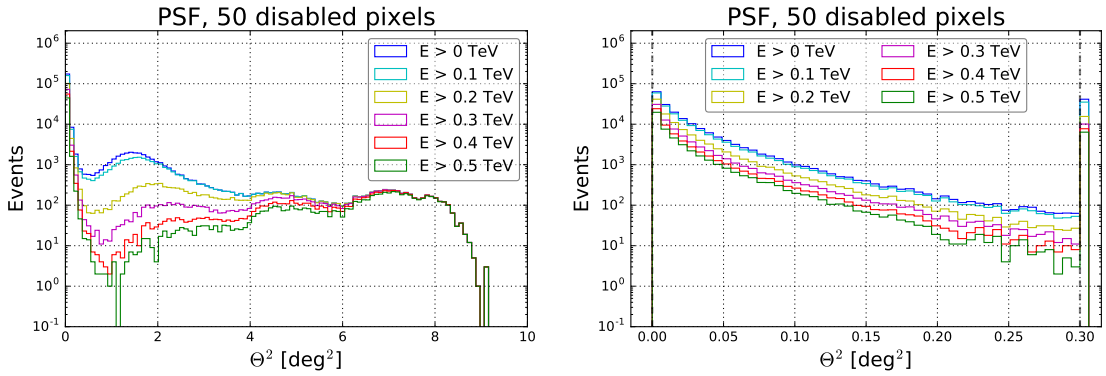

(a) Entire distribution.

(b) Distribution close to the source position.

Figure 3.7: Point Spread Function of the gamma simulations for 50 disabled pixels. The histograms differ in the minimal energy an event needs to be taken into account, from all events (0 TeV) to only events with an energy higher than 0.5 TeV.

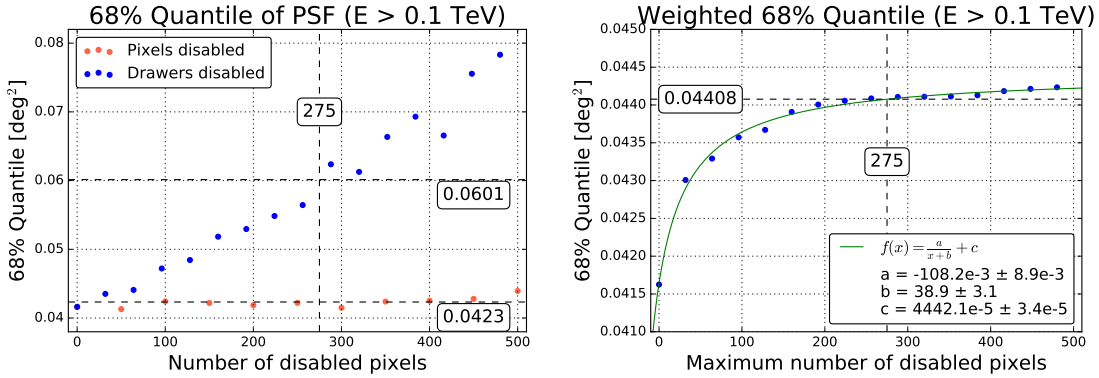

(a) Not weighted.

(b) Weighted with real distribution.

Figure 3.8: 68% Quantile of the PSF for an energy threshold of 0.1 TeV.

The weighting of the quantile was similarly done like for the relative energy bias. It can be seen in figure 3.8b. Here the same fit-function (eq. (4)) was taken and in table 3 the obtained fit values are displayed. The resulting more realistic value for the 68% quantile is $(44.08 \pm 0.05) \times 10^{-3}\,\mathrm{deg}^2$. The error here is calculated with eq. (12). The widening here is $\sim$**6%**.

The degradation of the efficiency and the 68% quantile for a broken pixel cut of 275 pixels is acceptable. Because of that the new limit is reasonably good. Since no differentiation of the reason why a pixel is broken was set and the results look good it seems that the two broken pixel parameters (hardware and HV switched off) can be combined to one criteria.

Parameter	**Type**	m	t
Relative energy bias	pixel	$(-3.77 \pm 0.06) \times 10^{-4}$	$(1.9 \pm 1.5) \times 10^{-3}$
	drawer	$(-3.30 \pm 0.07) \times 10^{-4}$	$(2.5 \pm 1.9) \times 10^{-3}$
Normalized efficiency	pixel	$(-5.89 \pm 0.10) \times 10^{-4}$	1.003 ± 0.0028
	drawer	$(-5.79 \pm 0.26) \times 10^{-4}$	0.996 ± 0.008
68% Quantile of the PSF	pixel	$(3.2 \pm 1.0) \times 10^{-6}$ [deg^2]	$(414.4 \pm 3.0) \times 10^{-4}$ [deg^2]
	drawer	$(74 \pm 4) \times 10^{-6}$ [deg^2]	$(39.7 \pm 1.0) \times 10{-}3$ [deg^2]

Table 2: Fit parameters of the linear fit (eq. 2) to the given quantity.

Parameter	a	b	c
Relative energy bias	0.93 ± 0.12	67 ± 8	$(-13.6 \pm 0.4) \times 10^{-3}$
Normalized efficiency	0.80 ± 0.12	28 ± 4	0.9709 ± 0.0006
68% Quantile of the PSF	$(-108 \pm 9) \times 10^{-3}$ [deg^2]	39 ± 4	$(4442 \pm 4) \times 10^{-5}$ [deg^2]

Table 3: Fit results of the weighted parameters, fitted with eq. (4).

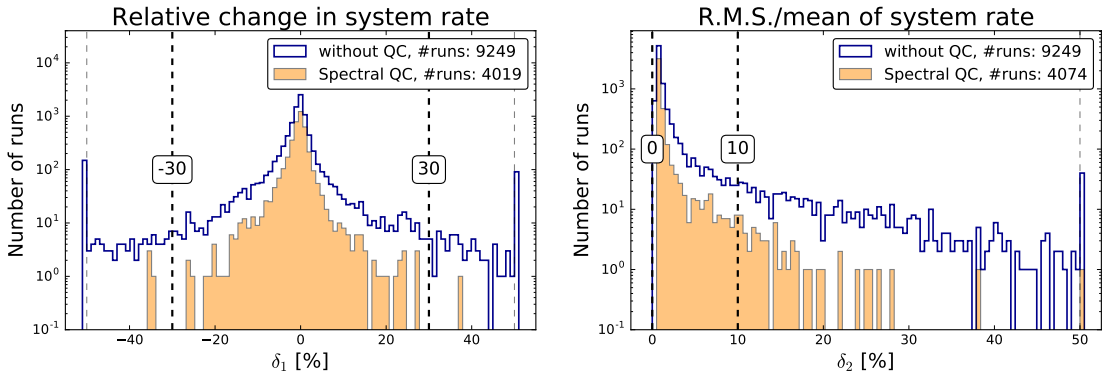

Figure 4.1: Spectral parameter distribution for CT5. The step histogram (blue) shows all runs without quality cuts. In the filled histogram (orange) all runs are counted which fulfill all spectral quality cuts, except the cut on the plotted parameter. The dashed lines with numbers indicating the position show the currently used limits on the given parameter. The thin gray dashed lines (without numbers) show the limit of the histogram. The bins outside of the thin lines are under- and overflow bins.

4. Spectral Criteria for H.E.S.S.-II

For this section the main task is the calculation of the TC for H.E.S.S.-II, but also the two other spectral cut parameters δ_1 and δ_2 (see sec. 2.2) need to be checked if it is necessary to adjust them. In figure 4.1 the distribution of δ_1 and δ_2 for CT5, can be seen. Outliers in the distributions of these two parameters are already well filtered by the other criteria, they are thus not studied further. For the first phase of the instrument the TC had great influence on the quality of the data selection, but has not yet been calculated for H.E.S.S.-II. In the next section the theoretical part to calculate the TC will be explained and thereafter the results for CT5 will be presented.

4.1. Transparency Coefficient

To successfully trigger a shower-event the thresholds on different levels need to be fulfilled as defined in section 1.2. The following theory was taken from [7]. There are several factors, which can modify the trigger rate like the percentage of the pollution of the air. The zenith-corrected telescope trigger rate R can be approximated by the local proton spectrum ($f(E) = 0.096 \cdot (E/TeV)^{-2.70}/(TeV \cdot s \cdot m^2 \cdot sr)$):

$$R = \int_{E_0}^{\infty} dE A_{eff}(E) \cdot f(E) \propto \int_{E_0}^{\infty} dE A_{eff}(E) \cdot E^{-2.7} \propto E_0^{-1.7+\Delta}, \tag{5}$$

with E_0 the energy threshold on camera level and $A_{eff}(E)$ the effective area of the telescope. The factor Δ in the exponent is the result of the dependency on the energy of A_{eff}. The detectable image size n_{ph} is inversely proportional to the atmospheric attenuation η, the muon efficiency μ, and the mean PMT gain over the camera g as shown in figure 4.2. μ is a measure of the optical efficiency of the telescope and g is the factor with which the initial electron inside a PMT is reproduced. Further explanations of μ and g are given later in this section. Naturally the same holds for the minimum detectable image size n_{ph}^{min}. With the fact that the size of the Cherenkov cone grows with the initial energy of the γ-ray it follows that n_{ph}^{min} is proportional to the energy.

$$E_0 \propto n_{ph}^{min} \propto (\eta \cdot \mu \cdot g)^{-1} \tag{6}$$

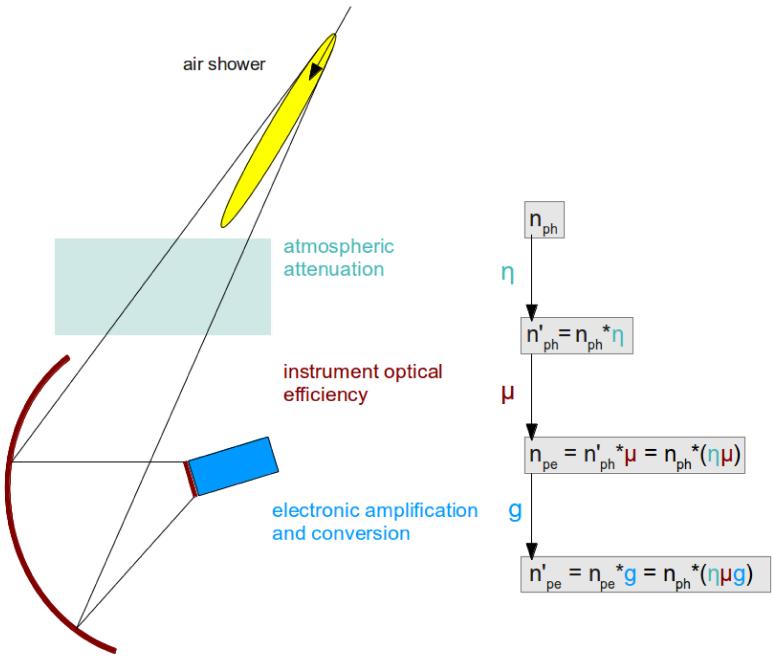

Figure 4.2: Schematic illustration of the effects weakening the Cherenkov signal. Image taken from [7].

The combination of eq. (6) with eq. (5) results in a relation for the atmospheric transparency.

$$\eta \propto \frac{R^{1/(1.7+\Delta)}}{\mu \cdot g} \equiv t$$

With the assumption $\Delta = 0$ the transparency coefficient t can be calculated by

$$t = \frac{R^{1/1.7}}{\mu \cdot g} \tag{7}$$

The correction of the trigger rate is necessary because the trigger rate is lower for larger zenith angles. In order to obtain a cut parameter which is valid for every run this needs to be taken into account.

Zenith correction

For larger zenith angles the Cherenkov photons have to travel a larger distance to the telescope. Because of that the probability of absorption becomes larger, thus the probability of seeing the showers decreases. The correction was done by fitting the data of trigger rate versus zenith angle, of all runs which fulfill the detection criteria with the new broken pixel cut for CT5 and with two additional constraints:

- RunNumber > 95000
- Zenith $\leq 90\,^\circ$

The constraint on the RunNumber is necessary because the high voltage supply of the CT5 camera has been adjusted at this time. For some runs the zenith angle is saved incorrectly and set to $99\,^\circ$. A zenith angle of $99\,^\circ$ would imply that the telescopes aimed under the horizon, consequently the zenith cut is needed. Moreover all runs which were taken on the Small Magellanic Cloud (SMC) are sorted out because for those runs the trigger rate shows an abnormality, which is discussed later. The used fit function is

$$f_{rate}(x) = a \cdot (1 + b \cdot (1 - \cos(x))^2), \tag{8}$$

where x stands for the mean zenith of a run. It is the same function which was used for the correction of the trigger rate for H.E.S.S.-I [4]. The corrected rate can be calculated by

$$R = \frac{r}{1 + b \cdot (1 - \cos(\phi))^2} \tag{9}$$

where ϕ is the mean zenith angle of the given run.

Mean gain
Inside a PMT the initial electron, which is released by the Cherenkov photon, is reproduced with a given factor called *gain*. This gain is determined in so-called calibration runs. The value is then averaged over the whole camera, which results in the mean gain g. For a given observation run the nearest preceding calibration run is used.

Muon efficiency
The muon efficiency μ represents the optical efficiency of the telescope. It is defined as the ratio of number of p.e. inside the shower image and number of photons reaching the mirrors. An event with enough information about the incident particle is needed to be able to calculate the theoretically detectable number of photons. This is the case for a muon event. These are seen as a ring on an image of an observation run. The number of photons, generated by muons, can be calculated from the ring radius and azimuthal intensity profile [5].
The confinement on the muon efficiency for the calculation of the TC is that only runs with a muon efficiency greater than zero are taken. A muon efficiency of zero would imply that no Cherenkov photons from a muon are detected. If this is the case, the muon is not detected and μ will not be calculated. Because of that $\mu = 0$ corresponds to a faulty calculation of the efficiency. Also the TC can not be calculated for $\mu = 0$.

The transparency coefficient criterion for the first phase H.E.S.S. was applied not telescope-wise, but applied to the whole run; the average of all active telescopes was taken. Since with H.E.S.S.-II mono analyses are performed, it is convenient to apply this cut only on the CT5 telescope for mono analyses, regardless of the other four telescopes.

4.2. Calculating the Transparency Coefficient

Before calculating the transparency coefficient the telescope trigger rate needs to be corrected for the zenith angle of the observation. As mentioned above, the fit function given in eq. (8) was used to describe the dependency of the trigger rate on the zenith angle. In figure 4.3 this fit is shown for CT5. As mentioned above the SMC runs show an abnormality, which can be seen by the difference between figure 4.3a (all runs are considered) and 4.3b (the SMC runs are excluded). The SMC runs have strong fluctuations in the trigger rate and form a vertical line at a zenith angle of $\sim 50\,^\circ$. Considering the resulting fit parameter b, these fluctuations have a large impact (see table 4). To see if this abnormality was also present for the smaller telescopes this fit was performed also for CT1-4. In figure 4.4 this is exemplarily displayed for CT3 and the same vertical line is seen. In figure 4.5 the rate as a function of the zenith angle is shown for different time intervals. Here it becomes visible that there are periods of time where the fluctuation of the rate is higher than for other times. In the appendix (see section C) all time periods are shown. The largest fluctuations occur roughly from August to October, but the exact intervals vary for every year. In the interval, where the SMC runs were taken the fluctuation is generally larger than at the other times. For simplicity, only the SMC runs were excluded from the fit here. For an removal of runs in particular time periods further studies would have been needed, to be sure not to remove too much acceptable data.
Another interesting fact which is visible considering the difference between figure 4.4b and

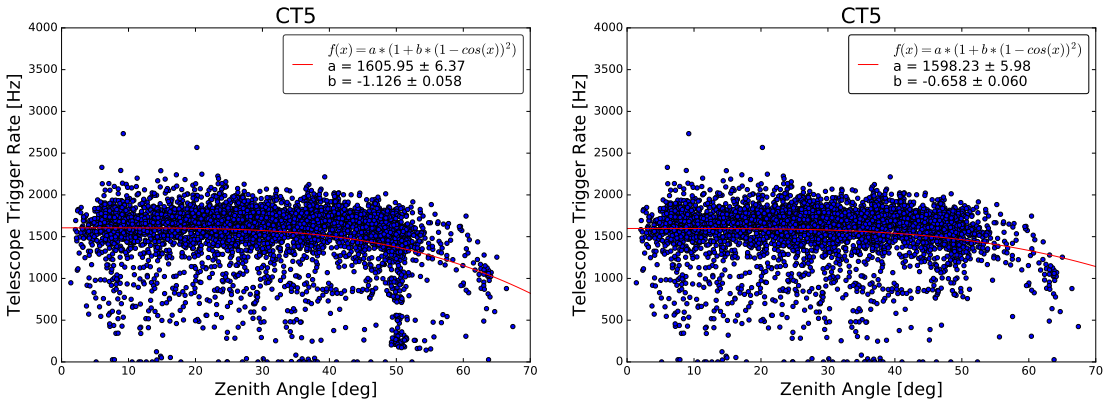

(a) All available runs.

(b) All runs except the SMC runs.

Figure 4.3: Rate vs. zenith fit of CT5 for the zenith angle correction.

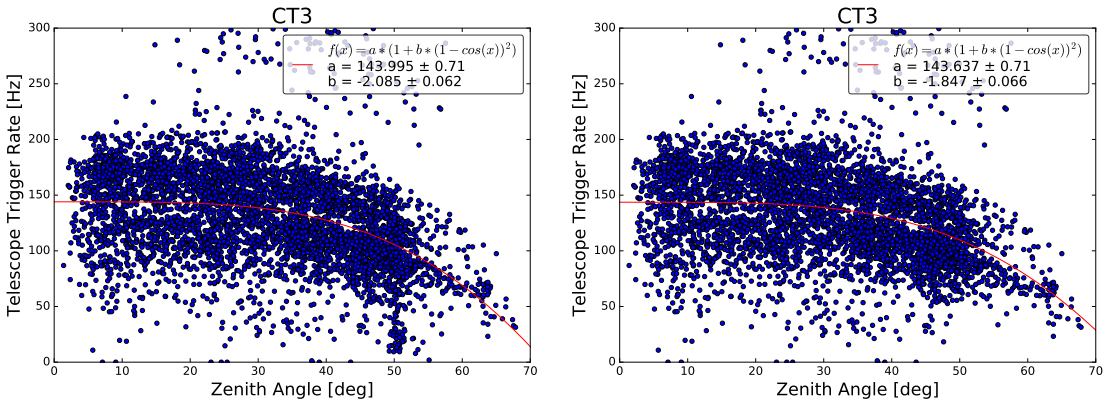

(a) All available runs.

(b) All runs except the SMC runs.

Figure 4.4: Rate vs. zenith fit of CT3. A stronger dependency on the zenith angle than for CT5 can be observed.

4.3b, is that the trigger rate of CT5 has a weaker dependency on the zenith angle than CT3. This holds true for all smaller telescopes, which can be seen in table 5. Here the fit parameters of all telescopes are shown, without the SMC runs. The factor b is the amplitude of the oscillation term in eq. (9). For the allowed range of the zenith angle between 0° and 90°, b determines how fast the rate decreases with the zenith angle. For lower values (CT1-4) it is declining quicker in comparison to higher values (CT5). This shows that the impact of the zenith angle on the trigger rate is greater for the small telescopes. With all necessary data the TC can be calculated with eq. (7). Its distribution for CT5 is shown in figure 4.6a. To be able to compare it with the H.E.S.S.-I result (fig. 4.6b), the peak is normed to one. Since the distribution for H.E.S.S.-I and H.E.S.S.-II look very similar, it is convenient to use the same limits for H.E.S.S.-II as in the previous phase of the telescope system.

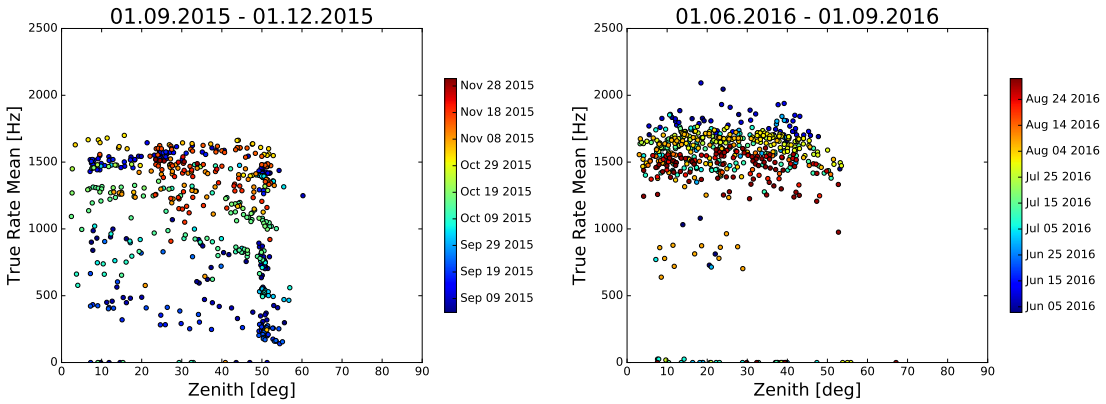

(a) High fluctuations.

(b) Low fluctuations.

Figure 4.5: Rate against zenith angle for CT5 for different time periods. The duration of a period is three months.

Runs	a [Hz]	b [Hz]
with SMC	1606 ± 7	-1.13 ± 0.06
without SMC	1598 ± 6	-0.66 ± 0.07

Table 4: Fit coefficients for CT5 for all runs and for all runs except the SMC runs.

Telescope	a [Hz]	b [Hz]
1	132.0 ± 1.1	-1.22 ± 0.11
2	141.0 ± 0.8	-1.63 ± 0.08
3	143.6 ± 0.8	-1.85 ± 0.07
4	140.6 ± 0.8	-1.57 ± 0.08
5	1598 ± 6	-0.66 ± 0.07

Table 5: Fit coefficients for the fit rate vs. zenith angle. For all runs except the SMC runs.

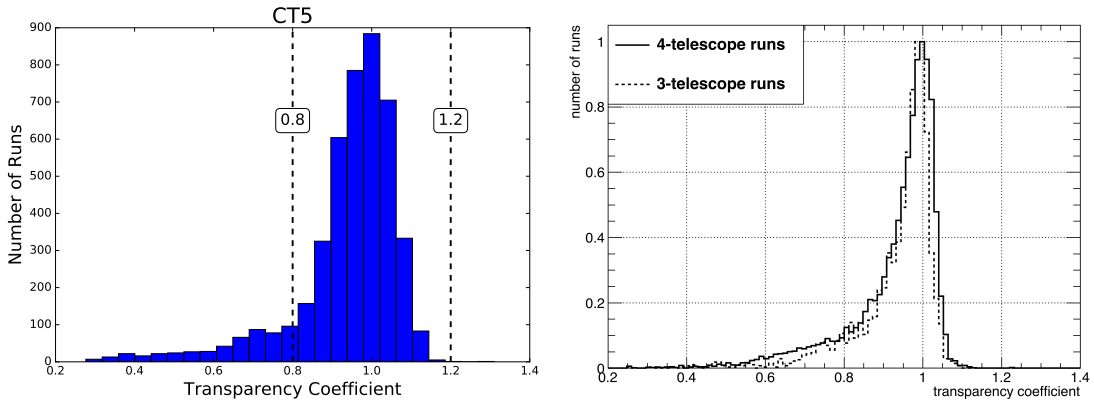

(a) Normed distribution for CT5. Dashed lines display the limits of the quality cut.

(b) Distribution for the first phase of H.E.S.S. from [7].

Figure 4.6: Transparency coefficient distributions.

5. Application of the Quality Selection to Data

In this section the effect of the quality selection on real observation data is studied. To do so, the flux of a source for which many observation runs are available is investigated. The flux is the number of events coming from the source per area and time. To calculate the flux of a source the *reflected background* method is used. For this a so called *on-region*, which contains the source, is defined. Also one or more *off-regions*, where no known sources are present, are chosen with the same size and shape as the on-region. Furthermore have the off-regions the same offset to the observation position, which is different to the position of the source. To avoid contaminations of the background estimation by outliers of reconstructed γ-rays, the area close to the on-region is avoided. For further information about the reflected background method see [2]. The number of events in the off-regions are averaged and then subtracted from the number of events counted in the on-region.
It was looked at the flux of the Crab Nebula because it has a high flux compared to other known TeV sources and the flux is known to be stable [1]. Thus a narrow distribution is expected. A mono analysis was carried out to obtain the flux. The constraint on the used runs was that the run number must be greater than 95000 because the high voltage supply of the CT5 camera has been adjusted at this time. In figure 5.1 the flux is shown for observations filtered by no quality cuts ("without QC"), detection cuts ("Detection QC"), and spectral cuts ("Spectral QC"). The bins to the left and right of the dashed lines denote the under- and overflow bins, respectively. In these bins every value outside of the histogram is stored. The negative flux values in the underflow bin are possible, if through a statistical fluctuation the rate in the background is higher compared to the rate in the on-region.
In table 6 the mean flux values with their standard deviations are shown for all three histograms. Large values compared to the mean flux values, in particular values larger than 4.5×10^{-11} cm^{-2}s^{-1}, are already well filtered out with the detection cuts. This verifies that the detection criteria set excludes runs with poor quality. The spectral cuts reject mostly runs with lower flux, specifically with flux values lower than the mean flux value. This is reasonable considering the distribution of the TC and its cut. Here mainly runs with low TC values are rejected. Therefore the atmospheric transparency was too low for these runs and thus fewer events were seen and lower fluxes are calculated.
The fact that the error on the flux for no quality criteria is so large is because of the values which lie outside of the range of the histogram and are only shown in the under and overflow bins. A similar distribution was made for H.E.S.S.-I in 2006. Here the distribution was centered at $(2.21 \pm 0.06_{stat}) \times 10^{-11}\mathrm{cm}^{-2}\mathrm{s}^{-1}$ and had a width of $(3.58 \pm 0.6_{stat}) \times 10^{-12}\mathrm{cm}^{-2}\mathrm{s}^{-1}$, which was obtained from a Gaussian fit [1]. The sigma is comparable with the obtained standard deviation for the mono analysis, which is a measure of the width of the distribution. Possible reasons why the width of the old analysis is smaller, are for instance, the analysis was performed in stereo mode and additional cuts were made on event level. All cuts can be looked up in [1]. Considering the mean flux values of the CT5 mono analysis it is clear that for every quality step from no selection to spectral criteria the difference to the mean flux of the H.E.S.S.-I stereo analysis becomes smaller. This shows that the detection and spectral criteria fulfill their purpose of increasing the quality of the selected data.

Quality	**Mean Flux** $[\times 10^{-11}\mathrm{cm}^{-2}\mathrm{s}^{-1}]$
without QC	3 ± 8
Detection	2.0 ± 0.9
Spectral	2.1 ± 0.9

Table 6: Mean value of the obtained flux distributions with standard deviations.

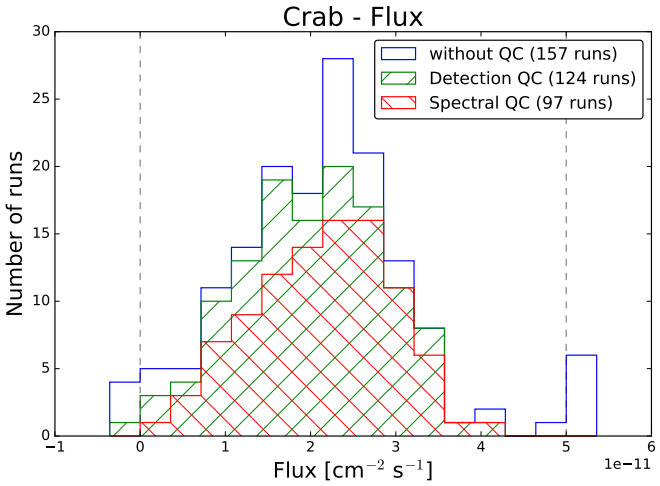

Figure 5.1: Distributions of the flux values of the Crab Nebula with no quality cuts ("w7o QC"), detection cuts ("Detection QC), and spectral cuts ("Spectral QC"). The dashed lines enclose the normal bins of the histogram. The two bins outside are the underflow (left) and the overflow (right) bins, which are filled with all data outside of the dashed lines.

6. Conclusion

In this thesis the quality selection of the data of H.E.S.S.-II was investigated and the transparency coefficient, which is a measure for the opacity of the atmosphere, was calculated for CT5. It became apparent that most of the limits on the criteria used for H.E.S.S.-I can also be used for the second phase of the telescope without adjustments. The parameters which showed the need to be studied were the broken pixel criteria and the duration. Since the reason for the cut on the duration was to assure sufficient statistics it was not modified. With the help of simulations of γ-ray events a new limit for the broken pixel criterion was found. The cut was set by the requirement that the energy bias should not become worse than 10%. The resulting limit was 275 pixels. This limit was proven to be reasonable through the validation by the efficiency and the 68% quantile of the PSF. Also there seems no need to separate the broken pixels because for this analysis no differentiation was done and the result looks reasonably good. But this can be investigated in the future with the help of observation data. One idea can be that for different causes of broken pixels, the mean number of joined broken pixels varies. The most common localization of the broken pixels on the camera may also change for different causes.
For the TC it seems reasonable to use the same limits as for the first phase of the telescope because the distributions of the TC for H.E.S.S.-I and H.E.S.S.-II look very similar. A topic which can be further looked at is the dependency of the trigger rate of CT5 on the zenith angle because for the small telescopes this dependency is clearly more visible. This can be done by looking at the time dependency in greater detail. Another issue is the calculation of the TC for stereo analyses. The TC for all telescopes need to be calculated and averaged for a run. The new broken pixel cut and the calculated TC were tested by the flux of the Crab Nebula. The quality criteria sets showed adequate effect on the distribution of the flux.
The main result of this thesis is the new broken pixel limit for the CT5 camera, which is set to 275 pixels. This cut in combination with the currently used cuts, can be used for H.E.S.S.-II analysis to achieve favorable data quality.

A. Detection Parameter Plots

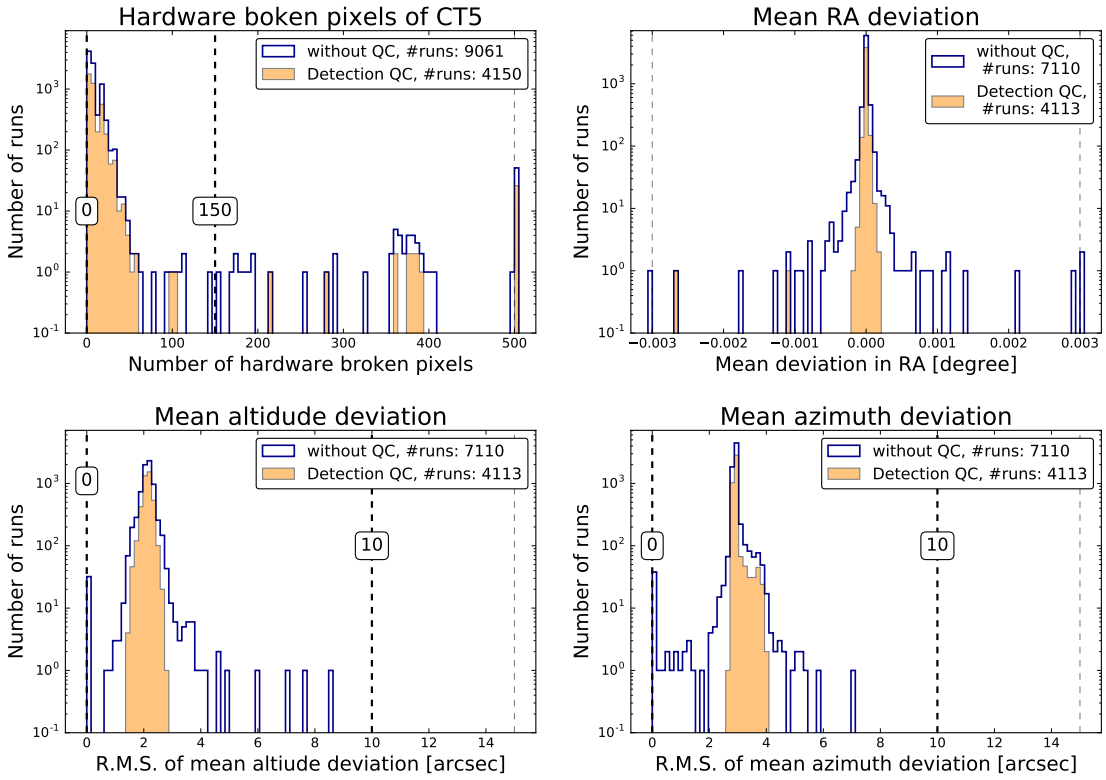

Figure A.1: Remaining detection parameter distributions of H.E.S.S.-II runs. The step histogram (blue) shows all runs without quality cuts. In the filled histogram (orange) all runs are counted which fulfill all detection quality cuts, except the cut on the plotted parameter. The dashed lines with numbers indicating the position show the currently used limits on the given parameter. The thin gray dashed lines (without numbers) show the limit of the histogram. The bins outside of the thin lines are under- and overflow bins. For the plot on the top right no lines which show the limits are seen, because the limits are out of the range of the plot.

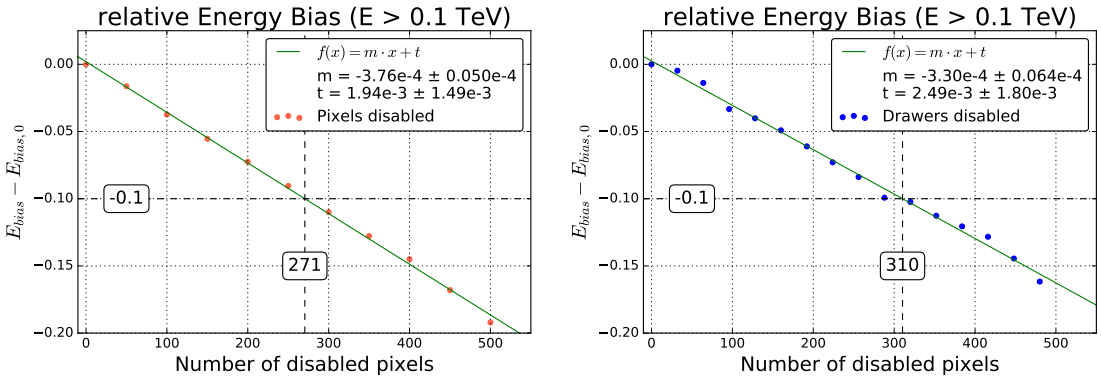

(a) Disabled pixels. (b) Disabled drawers.

Figure B.1: Linear fit to the relative energy bias.

B. Fits

B.1. Unweighted Quantities

The two errors resulting from the linear fit function (eq. (2)):

$$\Delta x = \sqrt{\left(-\frac{1}{m}\Delta t\right)^2 + \left(\frac{-0.1 - t}{m^2} \cdot \Delta m\right)^2} \tag{10}$$

$$\Delta f(x) = \sqrt{(x \cdot \Delta m)^2 + \Delta t^2} \tag{11}$$

with Δm and Δt the uncertainty of the fit parameters (see tab. 2).

B.2. Weighted Quantities

The error for the fractional fit function (see eq. 4):

$$\Delta f_{fraction}(x) = \sqrt{\left(\frac{1}{x+b} \cdot \Delta a\right)^2 + \left(-\frac{a}{(x+b)^2} \cdot \Delta b\right)^2 + \Delta c^2} \tag{12}$$

where Δa, Δb, and Δc are the errors of the fit parameters shown in table 3.

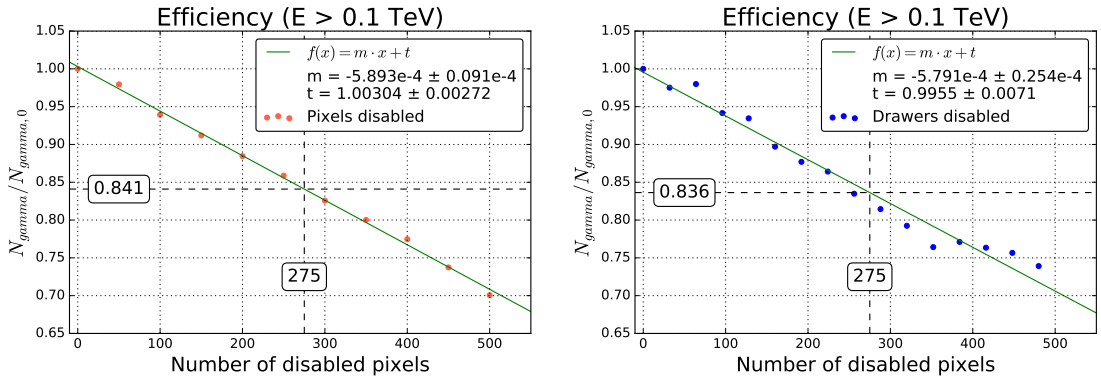

(a) Disabled pixels. (b) Disabled drawers.

Figure B.2: Linear fit to the normalized efficiency.

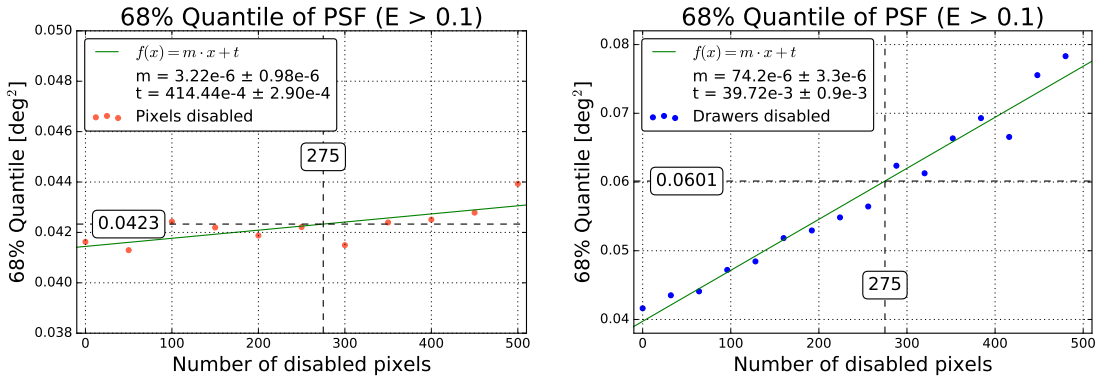

(a) Disabled pixels.

(b) Disabled drawers.

Figure B.3: Linear fit to the 68% quantile of the PSF.

C. Rate versus Zenith Angle

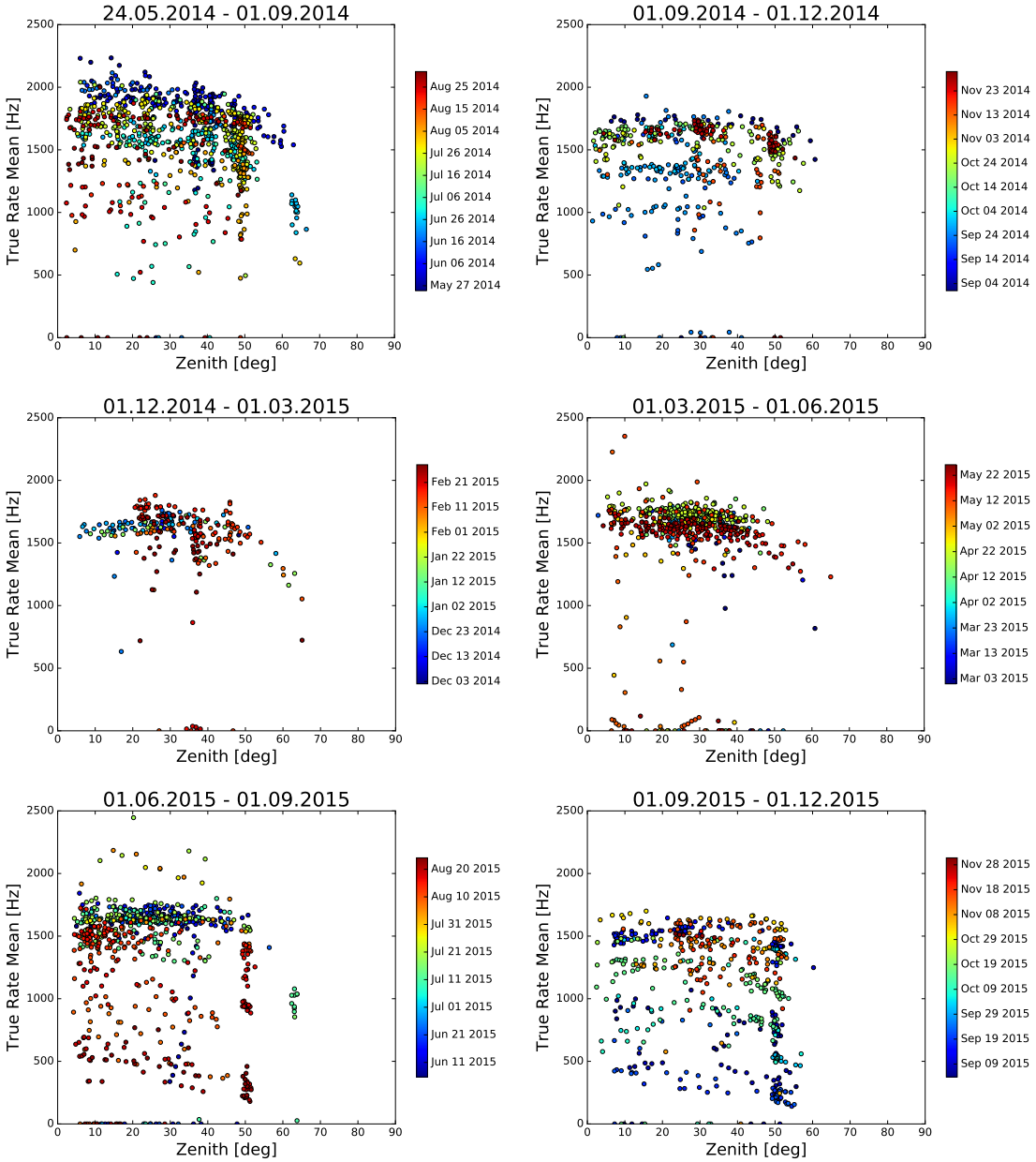

Figure C.1: Time resolved trigger rate versus zenith angle for CT5. Time period is 3 months.

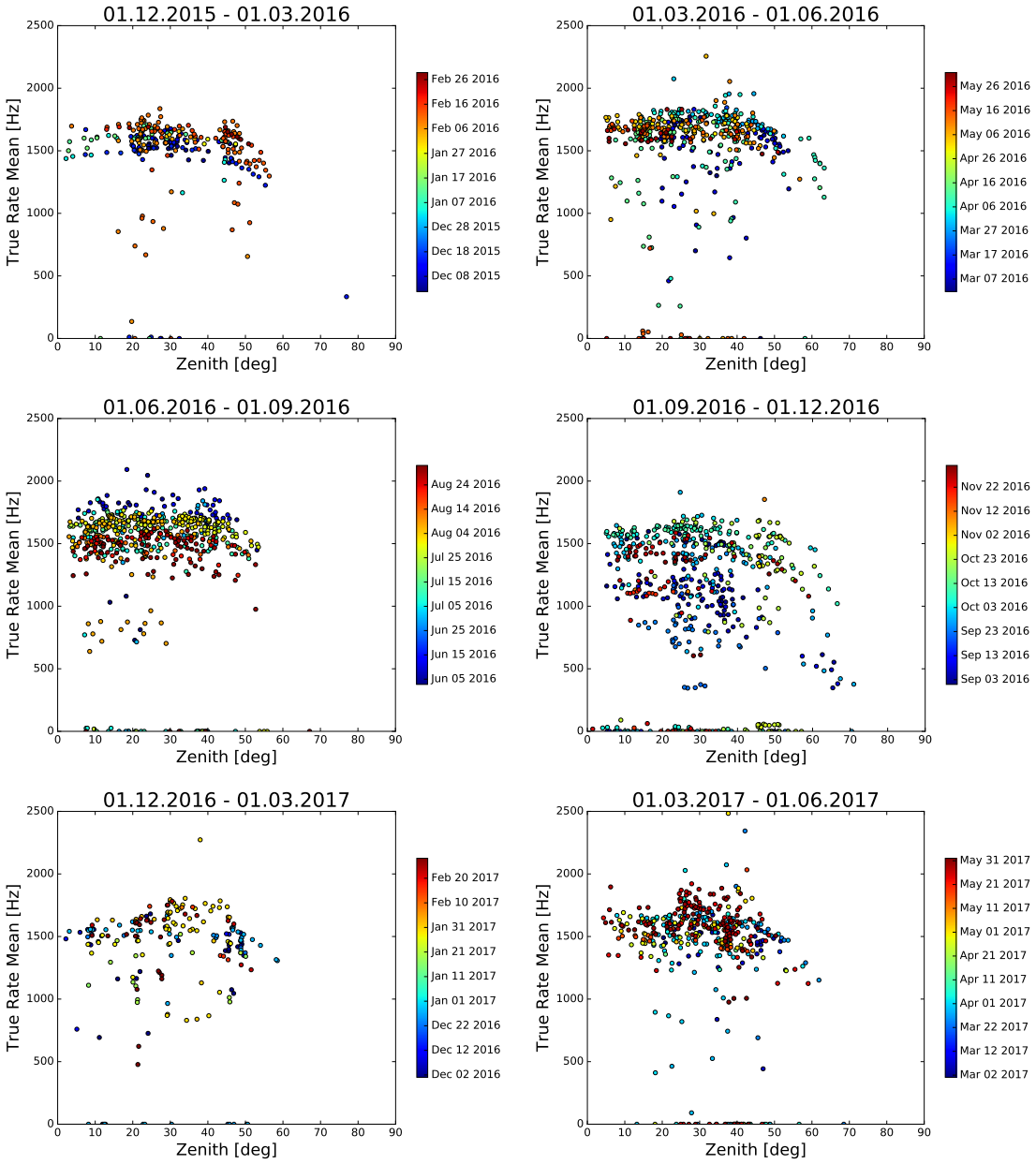

Figure C.2: Time resolved trigger rate versus zenith angle for CT5. Time period is 3 months.

References

[1] F. Aharonian et al. Observations of the Crab Nebula with HESS. *Astronomy & Astrophysics*, 457(3):899–915, Sept. 2006.

[2] D. Berge, S. Funk, and J. Hinton. Background modelling in very-high-energy γ-ray astronomy. *Astronomy & Astrophysics*, 466(3):1219–1229, Apr. 2007.

[3] O. Bolz. *Absolute energy calibration of the imaging Cherenkov telescopes of the H.E.S.S. experiment and results of first observations of the supernova remnant RX J1713.7-3946*. PhD thesis, Ruprecht-Karls-University Heidelberg, 2004.

[4] M. de Naurois. 11 - Transparency Coefficient. `https://hess-confluence.desy.de/confluence/display/HESS/11+-+Transparency+Coefficient`. Accessed: 04.03.2018, HESS Internal report.

[5] C. Deil, V. Marandon, and M. de Naurois. Hess 1 muon efficiency, Sept. 2012. HESS Internal report.

[6] S. Funk. Ground- and space-based gamma-ray astronomy. *Annual Review of Nuclear and Particle Science*, 65(1):245–277, 2015.

[7] J. Hahn, H. Gast, R. de los Reyes, C. Deil, K. Bernlöhr, K. Kosack, V. Maradon, and P. Hofverberg. *Heidelberg Data Quality Selection*, Feb. 2013. HESS Internal report.

[8] W. Hofmann and C. van Eldik. Ein neues Fenster zum Kosmos. *Sterne und Weltraum*, pages 38–47, Mar. 2009.

[9] University of Nova Gorcia. Cherenkov Telescope Array. `http://www.ung.si/en/research/cac/projects/cta/`. Accessed: 23.02.2018.

Erklärung

Hiermit bestätige ich, dass ich diese Arbeit selbstständig und nur unter Verwendung der angegebenen Hilfsmitteln angefertigt habe.

Erlangen, 05.03.2018

Maximilian Schandri